

Mechanical Extrusion of the Plasma Membrane to Generate Ectosome-Mimetic Nanovesicles for Lung Targeting

Yahui Liu, Yuelei Ling, and Wanyi Tai*

Cite This: <https://doi.org/10.1021/acs.molpharmaceut.4c00927>

Read Online

ACCESS |



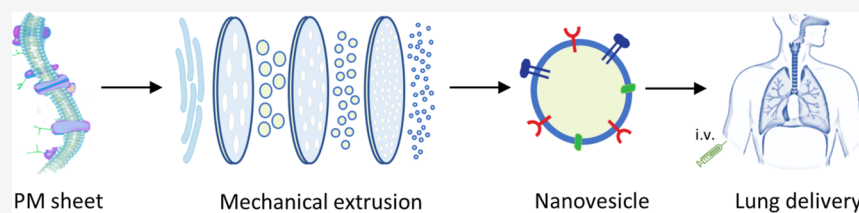
Metrics & More



Article Recommendations



Supporting Information



ABSTRACT: Extracellular vehicles (EVs) are naturally occurring nanocarriers that participate in the transportation of biologics between cells. Despite their potential in drug delivery, their optimal use in therapy remains a challenge, which comes from the difficulty in preparation scale-up and cargo loading efficiency. As a membrane-enclosed nanoscale system, EVs are reluctant to be transfected with cargos and purified by conventional methods. In the present study, we proposed an EV-mimetic nanovesicle system to overcome the challenges. Using the easy-culture mammalian cells as raw materials, we isolated the plasma membrane sheets and vesiculated them into membrane-enclosed nanovesicles as an EV mimic by the mechanical extrusion through porous membranes. In order to controllably load the cargos in the lumen of vesicles, the endogenous actin filament was chosen as an anchor to capture the cargos (fused with an anti-actin nanobody) in the inner leaflet of plasma membrane sheets and vesiculated inside after extrusion. By loading the bioluminescent tracer nano-luciferase (Nluc) and tracking biodistribution in mice, we unclosed the lung-tropic nature of these nanovesicles. Furthermore, we demonstrated that nanovesicles can be genetically engineered with chimeric antigen receptors to achieve the active targeting of lung cancer cells. In conclusion, our study indicated that plasma membrane extrusion might be an applicable approach to generate EV mimics for drug delivery, especially to the lung tissue.

KEYWORDS: extrusion, extracellular vesicle, plasma membrane, lung targeting, ectosome, EM-NV

INTRODUCTION

Extracellular vehicles (EVs) are membrane-enclosed nanoparticles secreted by many cells.¹ Based on their biogenesis, EVs can be categorized into two subtypes, known as exosomes and ectosomes. They were initially considered as waste carriers to eliminate cellular debris outside cells, but it was later found that EVs play important roles in cell-to-cell communication, having a natural capacity to transfer functional molecules (mainly protein, RNA, metabolite, and lipid cargo) between cells.^{2,3} The importance of EV-mediated communication has been documented in tons of literature, reflective of their diverse biological functions in the physiological and pathological processes of cells.⁴ As endogenous carriers, EVs feature an extraordinary delivery capability with low toxicity and immunogenicity, which has gained growing attention in the field of drug delivery.⁵ Various cargos, including siRNA, microRNA, mRNA, CRISPR ribonucleoproteins, and small-molecule drugs, have been packed into EVs and delivered to the recipient cells.^{6–10} Some formulations, for example, mesenchymal stromal/stem cell (MSC)-derived exosomes loaded with Ldlr mRNA (NCT05043181), KRAS^{G12D} siRNA (NCT03608631), and miRNA-124 (NCT03384433), have already entered phase 1 clinical trials.^{11,12} The disclosed results

from the pilot randomized clinical trials have revealed a good safety profile of exosome therapy in patients.^{13,14}

Despite the promising potential, the use of EVs in the clinical setting is restricted due to the lack of standardization in the preparation method.^{15–17} Due to the complex composition and small size, the EV samples in most studies were isolated directly from biofluids, either the blood serum or conditioned medium. However, these cell-derived EVs are generally a heterogeneous mixture of membranous vesicles comprising exosomes and ectosomes.¹⁸ Despite the similarity in functions, the subtypes are distinguished in aspects of lipid compositions, encapsulated cargos, surface proteins, and vesicle diameters owing to the difference of their biogenesis pathway.¹⁹ In addition, isolation of EVs is an inefficient, cumbersome, and time-consuming operation,²⁰ even when using the automatic ultrafast-isolation (EXODUS) systems.²¹ Singh's group

Received: August 18, 2024

Revised: November 18, 2024

Accepted: November 18, 2024

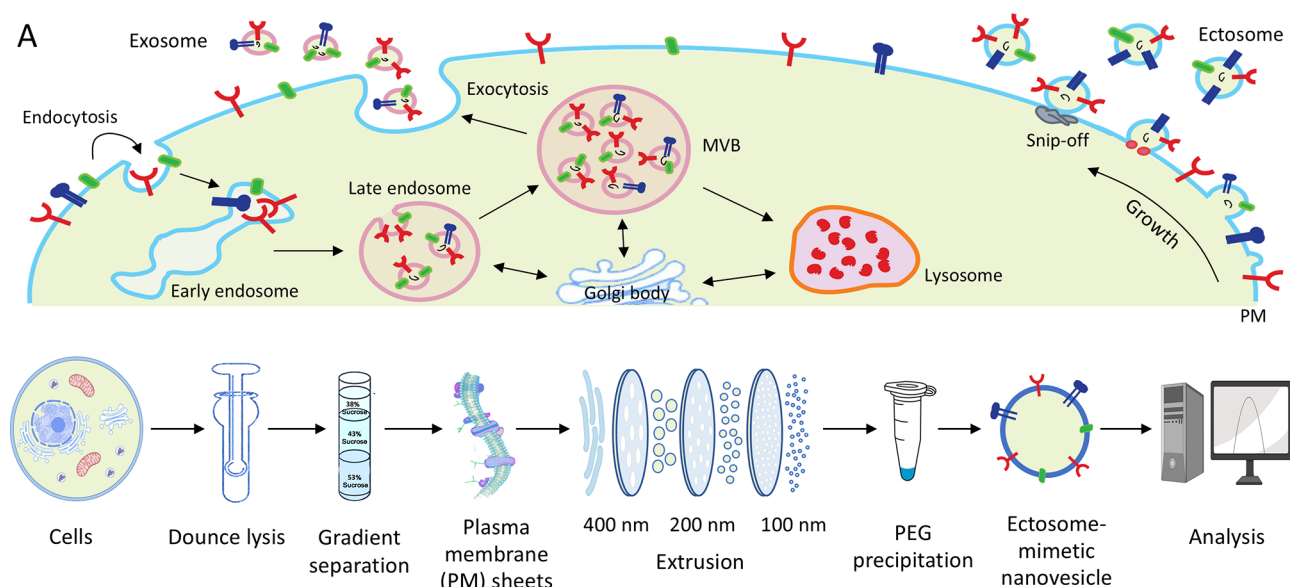


Figure 1. Generation of exosome, ectosome, and ectosome-mimetic nanovesicles. (A) Biogenesis of exosomes and ectosomes from cells. Biogenesis of exosomes began with the endocytosis of the PM proteins. This process involved invagination to form the intraluminal vesicles and finally maturing into intracellular multivesicular bodies (MVB). The MVB would either sort into a degradation pathway (lysosome) or proceed to release as exosomes into the extracellular space. Ectosomes were formed by the outward budding of the PM, followed by snip-off and release into the extracellular fluid. The diagram was adjusted from ref 19. (B) A scheme illustrating the preparation steps of ectosome-mimetic nanovesicles. Cells were homogenized, and the PM was isolated by discontinuous sucrose gradient centrifugation. After sequential extrusion through polycarbonate membranes with pores, the PM sheets were vesiculated into the membrane-enclosed nanovesicles. The ectosome-mimetic nanoparticles can be enriched by PEG precipitation for further analysis.

compared four isolation methods based on different principles. An average of around 100 μg of exosomes could be obtained from the 48 h-conditioned media of 3 million MiaPaCa cells.²² The yield was barely enough for several wells in SDS-PAGE analysis or probably one dose of mice tail-vein injection. The purity of the isolated EVs is another concern as various contaminations, including polyethylene glycol (PEG),²³ chemical precipitants,²³ albumin,²⁴ and lipoproteins,^{22,25} have been reported to co-isolate with EVs. Altogether, EV preparation faces various questions and challenges, especially when conforming with good manufacturing practices (GMP).

New approaches describing the exosome-mimetic nanovesicles or “reduced protocells” may overcome these shortcomings and offer insights for the large-scale generation of EVs.²⁶ Exosome-mimetic nanovesicles were produced by multiple extrusion of cells through filters of nanometer (nm) pore sizes.²⁷ The mechanical force deforms the cells in the nanosized pore channels and elongates the plasma membrane (PM), which forces it to vesiculate into the hollow nanovesicles consisting of cell membrane components.²⁸ The quantity of EVs produced in this method is 100 times more than the naturally secreted exosomes from the same number of cells.²⁹ Despite the high yield of the approach, plastic vesiculation from whole cells raises several questions. For example, other organelle membranes such as the nuclear membrane, Golgi membrane, and mitochondrial (Mito.) membrane may be integrated into vesicle shells during extrusion; the unwanted contents such as nuclear proteins and genomic DNAs may be encapsulated into vesicles as well; the extrusion-triggered cell death would activate bunches of proteases which may degrade the marker proteins. In this study, we optimized the approach to produce the nanovesicles by extruding the purified PM sheets instead of the whole cells. The PM is a nonliving part of cells that can be isolated,

purified, and stored on large scales. The nanovesicles produced from PM sheets are absent of contaminations from cellular components; meanwhile, the cargoes such as siRNA, drugs, and mRNA can be mixed with PM sheets and vesiculated inside the lumen during the extrusion process. Shingles et al. demonstrated the feasibility of this strategy by extruding the PM of erythrocytes into nanovesicles (diameter of around 100 nm) in the 1990s.³⁰ The erythrocyte membrane is a well-studied biological membrane, featuring its simple composition (lipids plus only two types of membrane proteins) and large elastic deformation capability (flexibility is essential when erythrocytes pass through narrow blood vessels). Here we expand the application by producing the nanovesicles from the PM of tumor and other immortalized cells, which we believe would better mimic the natural EVs of various sources. We demonstrated that the nanovesicles from cells of different origins well mimic the natural EVs in aspects of morphology, zeta potentials, and pharmacokinetics. We also found that the nanovesicles, as an EV mimetic, demonstrated high accumulation in the lungs, which may provide a new understanding of the targeting capability and therapeutic use of EVs.

RESULTS AND DISCUSSION

Generation of Nanovesicles by Extruding the PM Sheets. Despite the similarity in morphology, exosomes and ectosomes are two distinct types of EVs, which are separated on the basis of their biogenesis. The exosomes are released by the exocytosis of multivesicular bodies (MVBs) during lysosome maturation, while ectosomes are vesicles that bud outwardly from the PM (Figure 1A). We coin the nanovesicles of this study as ectosome-mimetic nanovesicles due to their origins of the PM. The nanovesicles were generated by stepwise-extruding the PM sheets, as depicted in Figure 1B. Due to the abundant availability of the cellular PM and scalable

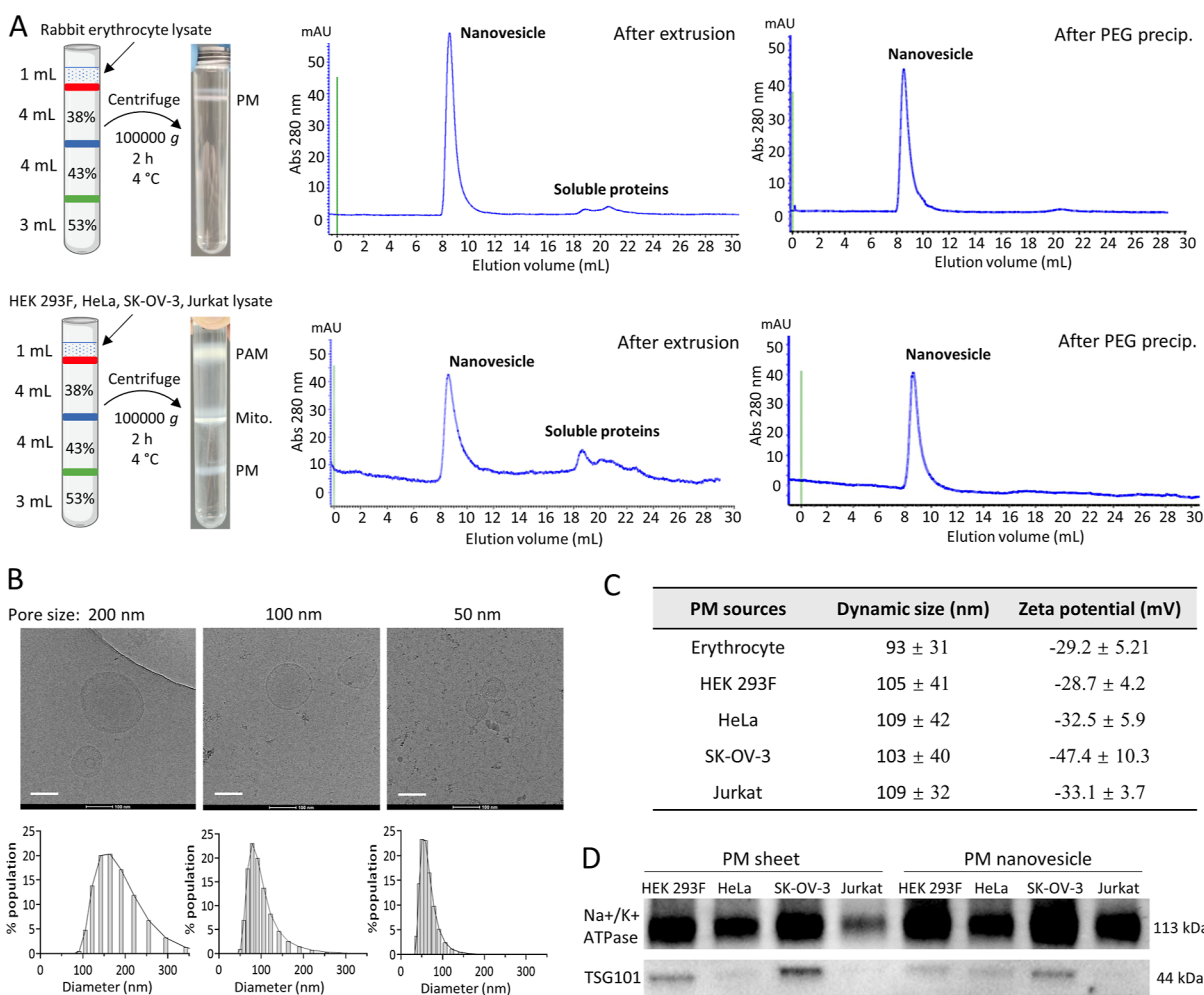


Figure 2. Preparation and characterization of ectosome-mimetic nanovesicles. (A) The stepwise characterization of nanovesicle preparation from either rabbit erythrocytes (upper panels) or HEK 293F (bottom panels). The crude membrane solution (1 mL) was laid on the top of a discontinuous sucrose gradient (38%, 43%, and 53%, from top to bottom). After ultracentrifugation, the PM fraction was collected and subject to mechanical extrusion to generate nanovesicles. The purity of nanovesicles was characterized by Superose 6 SEC chromatography after the extrusion and PEG precipitation steps, respectively. (B) Cryo-TEM images of nanovesicles after extruding the erythrocyte PM sheets through membranes of different pore sizes. The size distribution of vesicles is listed below accordingly. Scale bar, 100 nm. (C) A table showing the dynamic size and zeta potential values of nanovesicles extruded from different PM sources. (D) Characterization of EV marker proteins, Na⁺/K⁺ ATPase, and TSG101 on the PM sheets and corresponding nanovesicles.

technology for isolation, we aimed to establish a feasible method to prepare EV-like nanovesicles for drug delivery applications.

In order to generate ectosome-mimetic nanovesicles, we first sought to isolate and purify PM from cells. Density gradient centrifugation is the most popular method to separate the PM from other organelles in cell homogenates. It has been applied to prepare a highly pure PM from suspension cells, blood cells, and rat liver tissues in a scalable manner.^{31,32} As a pilot study, we first chose rabbit erythrocytes as a PM source because of their vast availability and anucleate feature. After lysis by the hypotonic buffer, erythrocyte fractures were placed on top of 38%–53% sucrose density gradients. The PM fraction was found to be located at the layer of 38% after ultracentrifugation (Figure 2A). The purified membrane sheets were extruded through polycarbonate membranes with 0.4, 0.2, and 0.1 μm pores sequentially for vesiculation into nanovesicles. This process was monitored by Superose 6 Increase size exclusion chromatography (SEC), which showed that the vesiculated nanoparticles were populated in a single sharp

(retention volume ~ 9 mL). Multiple minor peaks were presented at the retention volume of 18–22 mL, which could be assigned to the fractions of soluble proteins. In the next step, a PEG precipitation procedure was applied to remove these impurities. PEG precipitation is a routine operation to isolate exosomes or virus particles from media.^{33,34} It is applicable to purify and enrich the ectosome-mimetics nanovesicles in this study, as shown in Figures 2A and S1. Examination of the purified nanovesicles by cryo-TEM confirmed that they are closed vesicles devoid of membrane fracture (Figure 2B). Moreover, the vesicle size can be tuned by extrusion through membranes of specific pore sizes, although the number of extrusion cycles also affects the size distributions (Table S1).

Encouraged by the exciting results, we set out to generate nanovesicles from the PM of other cell origins. Four cell lines, including HEK 293F, HeLa, SK-OV-3, and Jurkat, were selected on the basis of biological diversity. Isolation of the PM was made according to the method described above, but Dounce lysis was adapted for these cells to rupture the

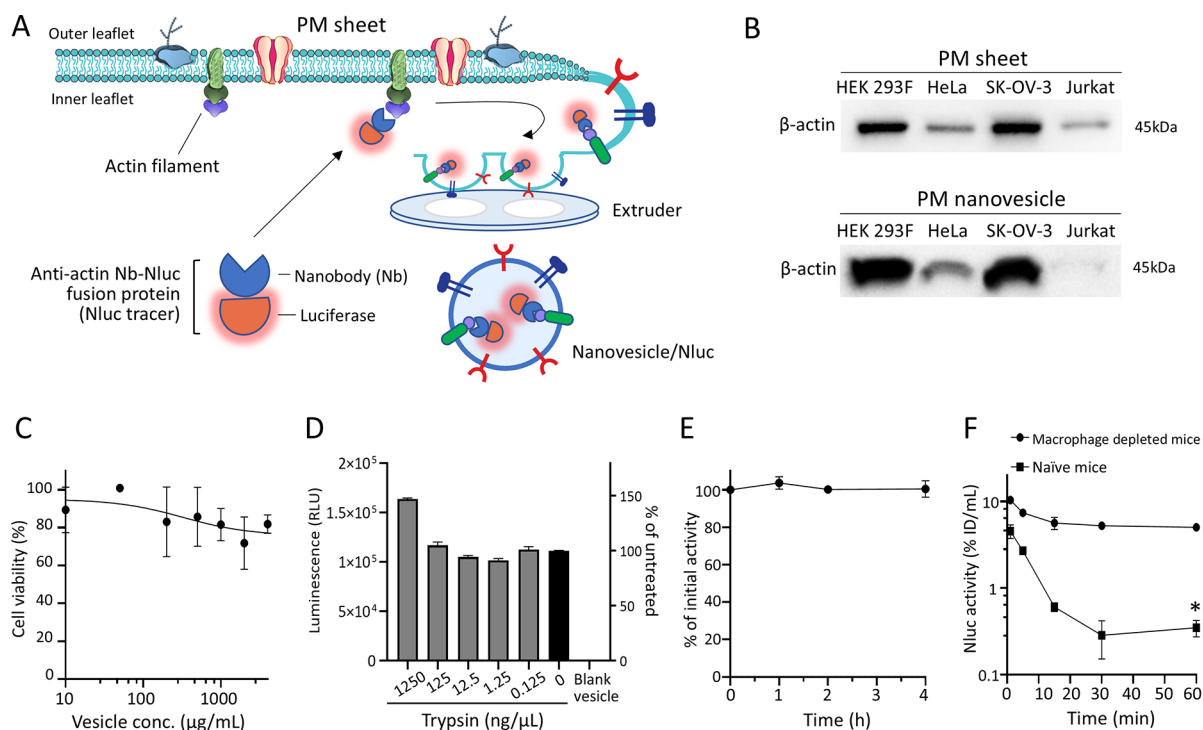


Figure 3. Loading of cargo into nanovesicles. (A) Scheme depicting the process of cargo (Nluc tracer) loading into the vesicle lumen. The Nluc tracer non-covalently binds to the actin filament in the inner leaflet of the PM sheet. The membrane vesiculates along the natural curvature and encapsulates the tracer inside the nanovesicle. (B) Western blotting analysis confirms the presence of beta-actin in the membrane sheets and nanovesicles. Each lane was loaded with lysates of equal amounts of total proteins (10 μg). (C) The viability of HEK 293F cells after treatment by serial dilutions of nanovesicle/Nluc. The vesicle concentration (conc.) is represented by the conc. of protein contents in vesicles (μg/mL). (D) After digestion of the surface proteins by trypsin, Nluc remaining inside vesicles was analyzed and compared. The relative luminescence activity was expressed as a proportion of the untreated control. (E) The stability of Nluc-bearing nanovesicles in 20% mouse serum. The activity was expressed as a proportion of the initial activity. (F) In vivo stability of Nluc-loaded nanovesicles in the blood circulation of naive mice and macrophage-depleted mice. Results are expressed as the mean of percentage of injected dose/mL ± SD ($n = 3$). * $P < 0.05$.

substructures.³¹ Different from the fraction obtained in the erythrocyte membrane, the density gradient centrifugation fractionated the crude membrane of these cells into three bands, which could be assigned to PAM (top band), mitochondria/ER (middle band), and the purified PM (bottom band), respectively (Figures 2A and S2). The PM fraction of the bottom band was collected and subjected to several rounds of extrusions following the procedures above. It is gratifying to see a major peak of nanovesicles in the chromatography of SEC. The retention volume of this peak is same to the one observed in the SEC of erythrocyte-derived nanovesicles (Figure 2A) and also in good agreement with the report by Vickers et al., who characterized exosomes using the same SEC method (Superose 6 increase 10/300 GL).³⁵ By expanding the procedures to other cell lines, we successfully obtained all the ectosome-mimetic nanovesicles of different cell origins. Nanoparticle size analysis showed that all of the nanovesicles exhibit a similar size distribution with a peak diameter of approximately 100–110 nm (Figure 2C), which is consistent with the observation in cryo-TEM (Figure S3). Despite the similarity in size and morphology, it is interesting that the nanovesicles of different cell origins could be distinguished from each other by zeta potentials, which might stem from the difference in their membrane-protein composition and glycosylation status. In addition, some marker proteins, including Na⁺/K⁺ ATPase and beta-actin, are present in the PM sheets and corresponding nanovesicles (Figure 2D). However, exosome-specific markers like TSG101, a protein

that originates from the endosomal compartment, are barely seen. These results demonstrated that nanovesicles of different PM sources could mimic EVs, especially ectosomes, in aspects of size, morphology, and protein contents.

Controlled Loading of Bioluminescent Tracers into the Vesicle Lumen.

As an endogenous carrier, EVs demonstrate great promise for the delivery of various cargos and drugs to the recipient cells. However, efficient loading of cargo inside EVs remains a challenge, despite several approaches such as electroporation, sonication, freeze–thaw cycling, and cell transfection for directly sorting cargo into exosomes, have been developed to facilitate cargo loading.¹⁷ Take siRNA, for example, based on mathematic calculation, Professor Schifferers assumed that the maximal loading efficiency of siRNA into exosomes by electroporation would likely achieve only 1 molecule of siRNA per 10 exosome particles when using 1 μg of siRNA per cuvette of electroporation.³⁶ It may leave room for improvement by optimizing the siRNA concentrations and electroporation conditions. However, in this regard, it is critically challenging to achieve reproducible and efficient loading of biological cargos into exosomes for clinical application. The difficulty comes from the fact that all of the EVs are membrane-enclosed systems that prevent cargoes from penetrating and being encapsulated. Our ectosome-mimetic nanovesicles are vesiculated from the PM sheets. These sheets are open and ready to encapsulate any cargo with which they interact.

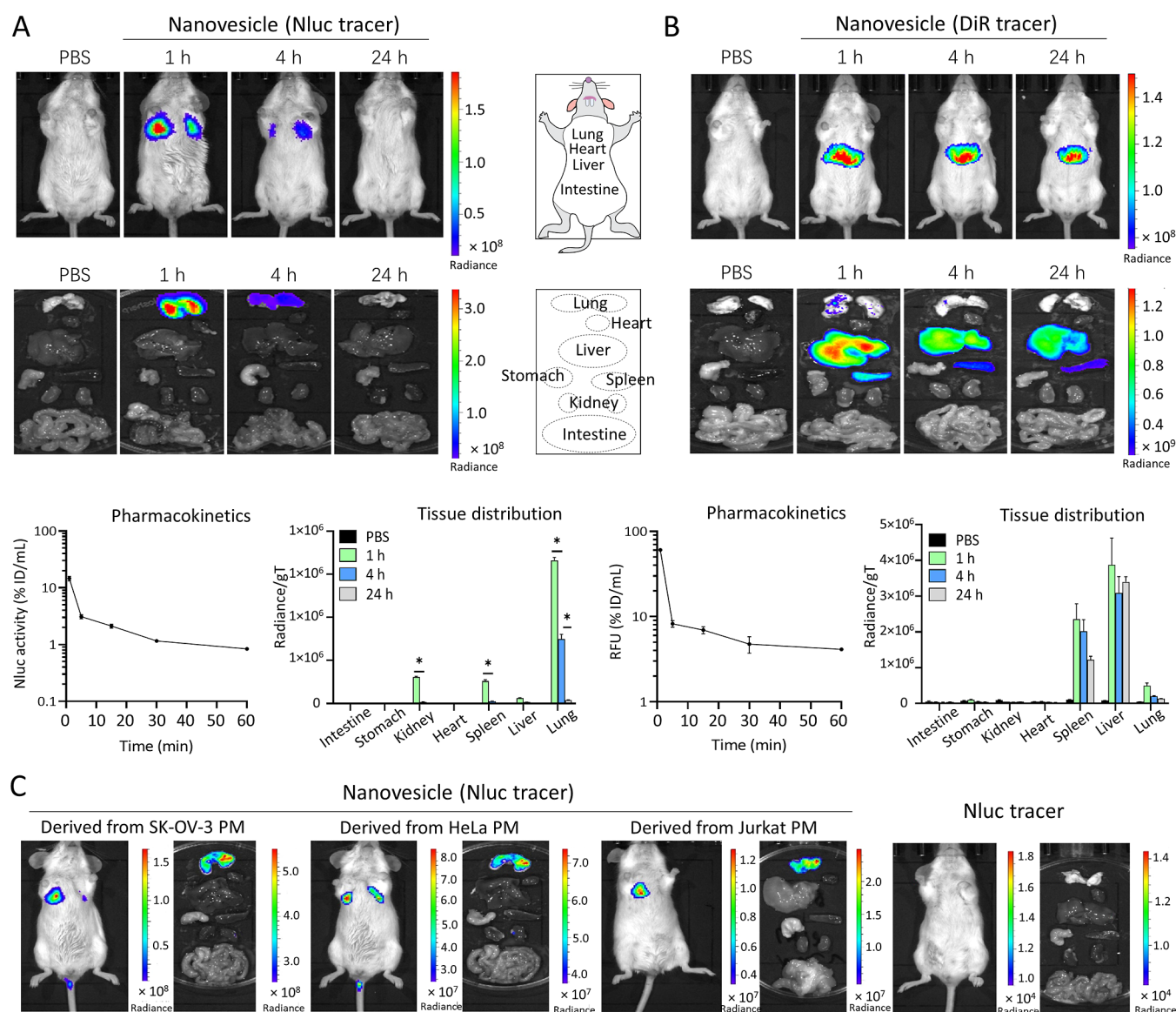


Figure 4. In vivo tracking and lung-tropic distribution of nanovesicles. (A) The real-time imaging of nanovesicle distribution in mice using bioluminescent tracer Nluc. After the in vivo live imaging (upper panel), the major organs were excised for ex vivo imaging (middle panel). Pharmacokinetics (bottom left) and quantitative analysis of distribution (bottom right) after tissue lysis were measured. ID, injected dose. RFU, relative fluorescence unit. * $P < 0.05$. (B) In vivo tracking of DiR-labeled nanovesicles in mice. The real-time live images, ex vivo images of excised organs, pharmacokinetics, and tissue distribution charts are listed in the upper, middle, bottom left, and bottom right panels, respectively. (C) In vivo imaging of Nluc-bearing nanovesicles derived from the PM of the other three cell lines. All the mice were intravenously injected with samples of equivalent amounts of protein contents. The images were taken 1 h after administration.

On the basis of this hypothesis, we attempted to load cargo inside the vesicle lumen using a protein–protein interaction approach (Figure 3A). More specifically, we conjugated the cargo with an anti-actin nanobody (Nb) and utilized it to help attach the cargo with the actin filament on the inner leaflet of PM by the antigen–antibody interaction. Once vesiculated by extrusion, the cargo will be encapsulated in the lumen of nanovesicles. One striking advantage of this loading method is that it would not affect the vesicles' topography including particle size and surface protein content. Beta-actin is an abundant protein in cells. It forms an actin filament network beneath the PM and supports the sketch of cells. Western blotting analysis in Figure 3B revealed that both the PM and nanovesicles contained beta-actin proteins, which proves that the actin filament was retained on the leaflet of the PM

membrane and could serve as an anchor for cargo loading. Here we chose NanoLuc luciferase (Nluc), a highly sensitive bioluminescent tracer, as a cargo and imaging tracer. It is genetically fused with the anti-actin Nb for controlled loading (sequence and characterization are available in Figure S4). There is no morphological difference between vesicles with and without the Nluc tracer. No cytotoxicity was found in cells treated with the Nluc-loaded nanovesicle (Figure 3C). However, after the addition of the luciferase substrate, the Nluc-bearing nanovesicles can generate a bright luminescence whose intensity is approximately 10^5 -fold higher than that of the blank nanovesicles, suggestive of successful Nluc loading (Figure 3D).

In the extruding process, the mechanical force might reverse the membrane curvature of PM and generate inside-out

nanovesicles. It is postulated that the Nluc tracer of inside-out vesicles should be located on the surface and thus be susceptible to degradation when the protease is added. The proportion of inside-out nanovesicles therefore can be determined by comparing the luminescence activity of Nluc nanovesicles in the presence or absence of protease treatment. As shown in Figure 3D, the luminescence activity of nanovesicles is almost consistent with the increase of trypsin concentration from 0.125 to 125 ng/ μ L. The result indicates that nanovesicles produced by extrusion largely have the right orientation of the membrane. It is noted that an aberrant increase in luminescence signal was observed when the trypsin concentration increased to 1250 ng/ μ L, which might be attributed to the nonspecific hydrolysis of substrates by trypsin.

Next, we examined the stability of Nluc nanovesicles in mouse serum. The vesicles bearing the Nluc tracer were incubated with 20% mouse serum at 37 °C. The nanovesicles were sampled at indicated time points, and their luminescence activity was compared to the initial activity of an equal number of Nluc vesicles. The result in Figure 3E shows that there was no signal decay even after 4 h of incubation, suggesting good stability in serum. The promising result prompted us to extend the stability evaluation to *in vivo* conditions. Nanovesicles carrying the Nluc tracer were administered into naïve mice with an initial dose (ID) of 10 μ g of vesicles (protein). Blood from the treated animals was collected, and the luminescence was measured. Figure 3F reveals that less than < 5% of ID/mL remained in blood at 15 min after administration. The sharp decline of activity over time indicated a short circulation half-life (< 5 min) of nanovesicles in mice. It is noted that the pharmacokinetics observed in this study is consistent with the previous report of exosomes which is eliminated quickly *in vivo* as well.³⁷ There is an ongoing appreciation that the EVs are cleaned systemically by the macrophages resident in tissues and circulation.³⁷ In order to determine whether the ectosome mimetic nanovesicles were also cleaned by the phagocytic system, mice were pretreated with clodronate liposomes to deplete macrophages and then administered with Nluc nanovesicles for blood kinetic analysis. A much slower decline of luminescence activity was observed in the blood of macrophage-depleted mice. The pharmacokinetic profiles in Figure 3F showed that the residual Nluc activity in the blood of these mice was approximately 14-fold higher than those of naïve mice at 1 h after administration. The result demonstrated that the nanovesicles, generated by mechanical extrusion, have a short circulation half-life and poor systemic stability, similar to those of natural EVs.

In Vivo Tracking and Lung-Tropic Distribution of Nanovesicles. We then explored the biodistribution of nanovesicles in mice using the Nluc tracer. Nanovesicles (100 μ g) derived from HEK 293F PM were administered into mice via tail-vein injection. The *in vivo* imaging was tracked at 1, 4, and 24 h after administration. The whole-body images in Figure 4A revealed that strong luminescence could be detected in the lungs, but the signal decreased gradually over time and was almost undetectable at 24 h. Surprisingly, no signal was detected in all other organs, including the liver. We speculated that the weak signal in other organs might be attributed to the poor penetration of bioluminescence because the Nluc emits the blue-light signal which has a short wavelength and poor penetration. The *ex vivo* imaging of the excised major organ did show signal enhancement, but the luminescence remains exclusively in the lung. An increase in the detection sensitivity

was achieved by quantitative analysis of tissue lysates. It showed that the Nluc signal could be also recorded in the kidney, spleen, and liver at 1 h after injection, but the intensity was 5.4, 6.4, and 26.7 times lower than that of the lung, respectively (Figure 4A, bottom right). Moreover, the signal decayed quickly in all organs, indicating the fast degradation of the nanovesicles *in vivo*. Altogether, the result demonstrated a lung-tropic biodistribution of the ectosome-mimetic nanovesicles, suggesting their potential in lung-specific drug delivery.

To circumvent the penetrating limitation during tracking, we labeled the nanovesicles using a fluorescent dye DiR and re-evaluated the biodistribution by near-infrared imaging. DiR is a lipophilic near-infrared dye and can be readily inserted into the lipid bilayer of EVs to achieve noncovalent labeling. Due to the superb sensitivity and feasibility of labeling, DiR has been widely used as a probe for the *in vivo* study of EVs. It is surprising that the distribution pattern of DiR-labeled nanovesicles is distinct from that of our observation using the Nluc tracer. As shown in Figure 4B, we observed that DiR-labeled nanovesicles were mainly accumulated in the liver, followed by the spleen and lung. This trend was confirmed by *ex vivo* imaging and lysate quantification. In addition, the fluorescence signal of DiR in all organs decayed much slower than the decline rate of the luminescence signal observed in Figure 4A. For example, fluorescence intensity was persistent in the liver for at least 24 h (~ 88% remaining) in comparison to only 3% left in the lung when using the Nluc tracer. Since both vesicles (DiR-labeled and Nluc-labeled) exhibited similar pharmacokinetic profiles ($t_{1/2}$ < 5 min), the long fluorescence retention by DiR nanovesicles is unlikely attributed to a continuous accumulation in organs over time, instead by slow degradation and clearance of the DiR probe in tissues. DiR is a Cy7 analogue bearing two octadecyl (C18) chains. These long-carbon chains can be inserted into the cell membrane, leading to long retention in cells. Compared to the protein-based Nluc tracer, the DiR probe is much harder to degrade and clean out, which may render a pseudophenomenon during *in vivo* tracking. In addition, the lipid nature of DiR may favor hijacking the lipid transport pathway and result in an accumulation in the liver. The prominent accumulation of EVs in the liver has been reported by many groups when using DiR as the probe.^{38,39} It has long been questioned whether it reflects the real distribution pattern of EVs because the liver deposition might be the consequence of dye shedding off from vesicles or the alteration of the vesicle surface by DiR insertion.⁴⁰ Practicality of the Nluc tracer in Figure 4A provides a new insight into the biodistribution profile of EVs and may be worth paying attention to. In this study, the Nluc tracer was labeled on the endogenous actin filaments and located in the inner space of nanovesicles, which ruled out the likelihood of tracer leakage or changing the repertoire of vesicle surface proteins. Based on this assumption, we speculated that the Nluc tracer-based bioluminescence imaging in Figure 4A might accurately reflect the distribution of EVs or EV mimetics *in vivo*. A similar pattern of lung-tropic accumulation of EVs has been previously reported using other luciferase-based fusion tracers.^{40,41} Moreover, it has been proposed that $\alpha 6\beta 1$ integrin is related to the lung distribution of melanoma-derived EVs.^{42,43} Takakura's group reported that ablation of the surface integrin $\alpha 6$ and $\beta 1$ by protease K treatment can attenuate the lung-tropic distribution of EVs.⁴¹ Despite some controversy, our result indicates that the

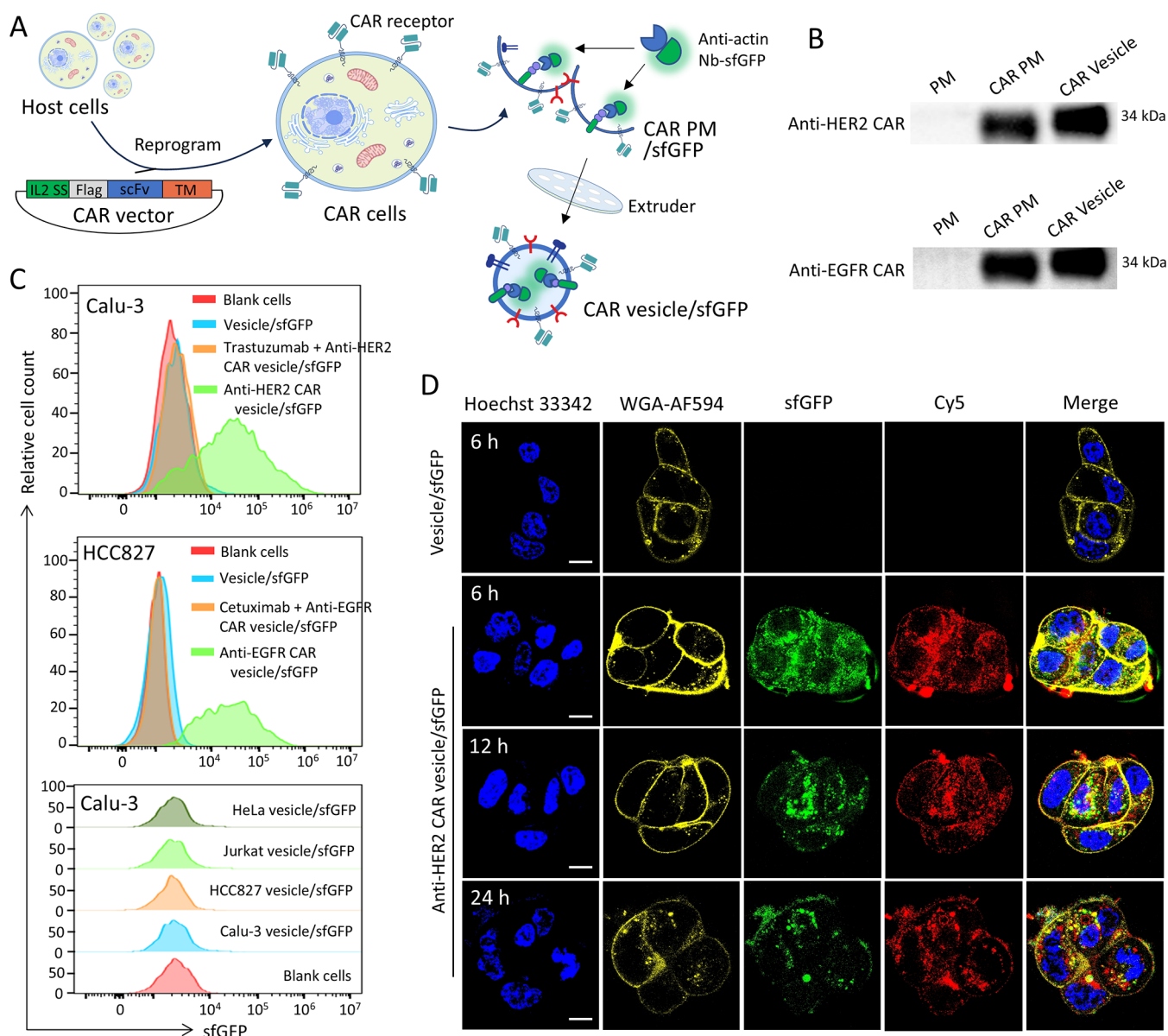


Figure 5. Active targeting of lung cancer cells by genetic engineering of nanovesicles with CAR receptors. (A) The generation process of CAR nanovesicles. The host HEK 293F cells were reprogrammed into CAR cells by transient transfection with the plasmid vector encoding the CAR gene. The PM was isolated as routine and vesiculated into nanovesicles after loading the sfGFP cargo (anti-actin Nb-sfGFP fusion protein). (B) Western blotting analysis of the CAR receptor proteins in CAR PM sheets and CAR nanovesicles. (C) Flow plots showing the binding ability of CAR nanovesicles to the corresponding antigen-overexpressing lung cancer cells. All the nanovesicles were labeled with the sfGFP tracer for detection. (D) Confocal images of the HER2-positive Calu-3 cells after treatment by sfGFP-labeled vesicles or anti-HER2 CAR vesicles at 37 °C over time. The nucleus was counterstained by Hoechst 33342, the cell membrane was stained with WGA-AF594, and the nanovesicles were labeled by the sfGFP tracer and sulfo-Cy5 NHS, respectively. Scale bar: 10 μ m.

ectosome-mimetic nanovesicles exert lung-tropic distribution and the encapsulated Nluc tracer might enable accurate spatiotemporal tracking in mice.

We further validated the lung-tropic distribution using nanovesicles derived from the PM sheets of other cell lines. In this experiment, we injected the same doses of different nanovesicles (100 μ g) into mice and compared their *in vivo/ex vivo* bioluminescence images with the control group of Nluc tracer alone (equivalent dose without the vesicle). The time point of imaging was chosen at 1 h after administration because of the high signal intensity. As shown in Figure 4C, nanovesicles from all three cell lines demonstrated the highest deposition in the lung, in comparison to other organs. The

lung-tropic trend was in agreement with the observation from HEK 293F-derived nanovesicles. By comparing the intensity of the luminescence signal in the lung tissue *ex vivo*, it was found that the nanovesicles display different signal intensities in the lungs, which is correlated to the abundance of beta-actin in vesicles and the corresponding capacity of Nluc loading (Figure S5). Altogether, we speculated that the tropism of lung tissue might be a natural feature of all EVs and EV mimetics considering the broad expression of integrins in mammalian cells.

Active Targeting of Lung Cancer Cells by Chimeric Antigen Receptors. The lung-homing potential of nanovesicles is exciting. Moreover, the active targeting by

genetically engineering vesicles could be implemented to increase their specificity to the lung's disease sites, i.e., lung cancer cells. Genetical engineering of exosomes has been reported to actively target tumor cells by tumor-homing peptides.⁴⁴ Here, we reprogrammed the host cells (HEK 293F) with the scFv-based chimeric antigen receptor (CAR) and extruded the CAR-bearing PM to generate the CAR nanovesicle for active targeting of lung cancer cells (Calu-3 and HCC827). The CAR is composed of an IL-2 signal sequence (IL2 SS) for the secretory pathway, the scFv domain specific to HER2 or EGFR receptors of tumor cells, and a CD8 α transmembrane (TM) segment sequence that anchors to the PM of host cells (Figure S6). We encoded the CAR in a plasmid vector and transiently transfected it into HEK 293F cells to display it on the extracellular side of the PM (Figure 5A). 48 h after transfection, cells were harvested for PM isolation. The CAR membrane sheets were labeled with an anti-actin Nb-sfGFP fusion protein (sfGFP tracer, Figure S7) and then vesiculated by mechanical extrusion. Western blotting was performed to detect the presence of CAR proteins using a monoclonal antibody against the FLAG tag (DYKDDDDK was encoded at the N terminus of the CAR). As shown in Figure 5B, high levels of anti-HER2 CAR (derived from trastuzumab) and anti-EGFR CAR (derived from cetuximab) were detected in the two CAR vesicles, respectively. Their presence in vesicles could also be traced back to the isolated membrane sheets from CAR cells.

Next, we assessed the targeting ability of two CAR vesicles to lung cancer cells Calu-3 and HCC827, respectively. As the flow plot shown in Figure 5C, the HER2-positive Calu-3 cells were recognized by anti-HER2 CAR vesicles but not the sfGFP-bearing vesicles without CAR (CAR-free vesicle). The same result was confirmed on HCC827 cells, too. It was surprising to find that the fluorescence intensity of Calu-3 cells treated with CAR-free vesicles (Vesicle/sfGFP) was comparable to that of the untreated cells, indicating that the nanovesicle itself has no affinity to lung cancer cells Calu-3. We further expanded the test to other CAR-free nanovesicles from different cell origins. None of them can bind the Calu-3 cells (bottom panel). Noncancerous HEK 293F cells have no interaction with these CAR-free nanovesicles as well (Figure S8). Interestingly, we did observe the lung-tropic feature of the nanovesicles in Figure 4. It might be explained that the recipient cells of CAR-free nanovesicles in lung tissues might be other cell types or subpopulations, even the extracellular matrix proteins, which is unknown. Nevertheless, it fosters the necessity of genetic engineering. In Figure 5D, confocal laser scanning microscopy was performed to track the uptake of anti-HER2 CAR nanovesicles on Calu-3 cells. After 6 h of incubation at 37 °C, the high uptake of anti-HER2 CAR vesicles to Calu-3 cells was observed, in comparison to the vesicles without CAR (loaded with the anti-actin sfGFP tracer), which is in agreement with the data of flow cytometry. With the increase of incubation duration, we observed a decay of vesicle fluorescence signals (sfGFP and Cy5), indicating the biodegradation of cargos. We further examined whether anti-HER2 CAR vesicles can specifically reach HER2-positive tumors in vivo. The Nluc tracer was encapsulated into the anti-HER2 CAR vesicles and injected into the Calu-3 tumor-bearing mice via the tail vein. The distribution of vesicles was visualized by luminescence imaging after administration of the Nluc substrate at 4 and 24 h postdose. The results in Figure 6A revealed that anti-HER2 CAR vesicles, but not the CAR-free

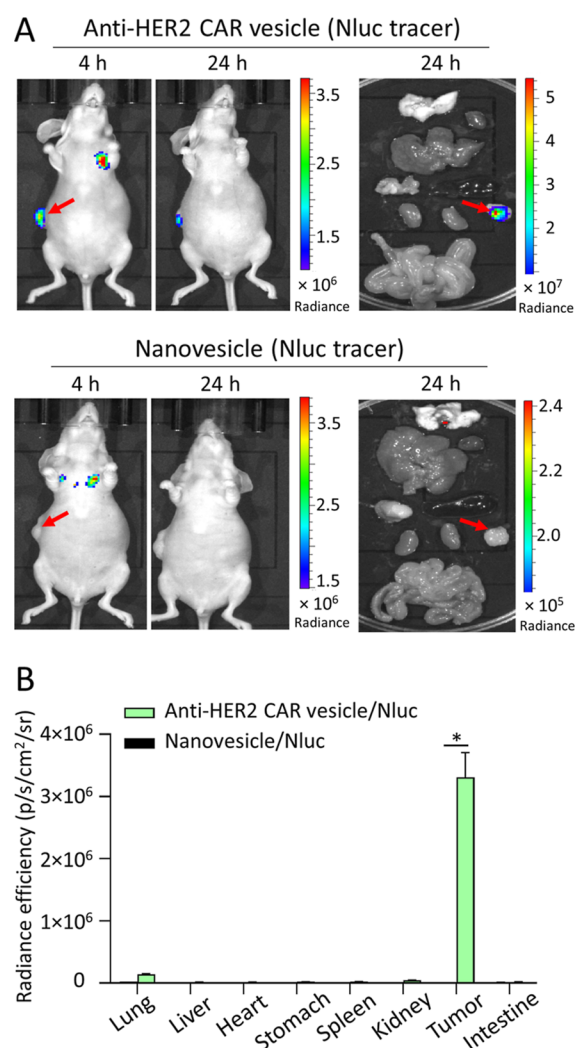


Figure 6. Distribution of anti-HER2 CAR nanovesicles in the lungs and HER2-positive Calu-3 tumors. (A) In vivo luminescence imaging of tumor-bearing mice over 4 and 24 h post-i.v. injection of anti-HER2 CAR vesicles or CAR-free nanovesicles (Nluc-labeled). Ex vivo images of organs and Calu-3 tumors were collected at the end point (24 h). The red arrows indicate the tumor sites. (B) Quantification of the luminescence radiance efficiency measured ex vivo in organs and solid tumors. * $P < 0.05$.

vesicles, can actively target the Calu-3 tumors. Both vesicles demonstrated lung-tropic distribution at 4 h after iv injection, but the deposition of anti-HER2 CAR vesicles was more persistent and significant in tumors (Figure 6B). Collectively, these results demonstrated that nanovesicles could be genetically engineered by CARs, and it promotes the specific delivery to the disease-related cells in the lung.

CONCLUSIONS

In summary, we have developed a method to generate ectosome-mimetic nanovesicles by mechanically extruding plasma membranes. These nanovesicles, either derived from erythrocytes, normal cells, or cancerous cells, retain the characteristics of EVs. Importantly, the new method allows us to controllably load cargos, such as sfGFP or luciferase, into the inner space of vesicles, which minimizes the alteration to the shell's topography and physiochemistry. With the aid of this advantage, we are able to tracelessly label the nanovesicles

with a Nluc bioluminescent tracer and track the biodistribution in mice, which helps us unclosethe lung-tropic nature of EVs. This study also demonstrated a potential to upgrade the nanovesicles with CAR for actively targeting lung cancer cells, which promotes the delivery of EVs to the lungs.

MATERIALS AND METHODS

Materials. The Roswell Park Memorial Institute (RPMI) 1640 medium, fetal bovine serum (FBS), and other cell culture supplementary reagents were purchased from Procell Inc. (Wuhan, China). The Union-293 expression medium was purchased from Union-Biotech (Shanghai, China). The mini-extruder and polycarbonate membrane filters with different pore sizes were obtained from Avanti Polar Lipids (Alabaster, USA). Kimble Kontes Dounce was ordered from Thermo-Fisher Scientific (Waltham, USA). Superose 6 Increase 10/300 GL column was purchased from Cytiva (Logan, USA). The antibodies trastuzumab and cetuximab were obtained from MedChemExpress (Shanghai, China).

Cell Lines. SK-OV-3, Calu-3, HCC827, HeLa, and Jurkat cell lines were maintained in RPMI 1640 medium supplemented with 10% FBS and 1% penicillin/streptomycin at 37 °C in 5% CO₂. HEK 293F cells were a kind gift from Dr. F. Long (Wuhan University, China) and maintained in the Union-293 expression medium with shaking at a speed of 110 rpm at 37 °C in 5% CO₂.

Cell Lysis and Density Gradient Purification of the PM. The erythrocytes were lysed according to the previous report.⁴⁵ Briefly, rabbit red cells were resuspended in hypotonic buffer (10 mM Tris-HCl, pH 7.4) at 4 °C for 30 min, then centrifuged at 17000g for 30 min at 4 °C to remove the internal contents. The procedure was repeated three times to obtain the empty rabbit red cells, which were then resuspended in PMRB buffer (5 mM Bis-Tris and 0.2 mM EDTA, pH 6.0) for later use. The PM of other mammalian cells was isolated according to a previous report.⁵ Briefly, cells (SK-OV-3, HeLa, Jurkat, HEK 293F, or CAR cells) were resuspended in IB-1 buffer (225 mM mannitol, 75 mM sucrose, 0.5% BSA, 0.5 mM EGTA, and 30 mM Tris-HCl, pH 7.4) and homogenized with Kimble Kontes Dounce by using gentle strokes at 4 °C until the majority of cells were disrupted. After centrifugation at 800g for 5 min at 4 °C, the supernatant was collected. The supernatant was then re-centrifuged at 17,000g for 1 h at 4 °C. The pellet was collected and resuspended with PMRB buffer. This is the crude PM solution, which can be further purified by density gradient centrifugation. A discontinuous sucrose gradient was created by layering sucrose solutions of different concentrations to a 14 mL thin-walled polyallomer ultracentrifuge tube: from bottom to top: 3 mL of 53% (w/w), 4 mL of 43% (w/w), 4 mL of 38% (w/w). The crude PM solution (1 mL) was applied on top of the 38% sucrose gradient solution and centrifuged at 100,000g for 2 h at 4 °C in a Beckman Optima XE-100 ultracentrifuge (Beckman SW41 rotor). The PM layer was carefully collected and diluted in DPBS. To remove the sucrose residues, the PM solution was re-centrifuged at 17000g for 1 h at 4 °C, and the pellet was collected and resuspended in DPBS. The purified PM in DPBS was stored at -80 °C until extrusion.

Nanovesicle Preparation by Extrusion. The PM was sequentially extruded through 400 nm (5 cycles), 200 nm (5 cycles), and 100 nm (21 cycles) polycarbonate membranes using a mini-extruder (Avanti, Catalog 610000). The obtained solution contained both nanovesicles and soluble proteins. To

remove the protein contaminations, the vesicles were precipitated with PEG according to reference with minor modifications.⁶ Briefly, the nanovesicle solution was mixed with an equivalent volume of PEG buffer (20% PEG8000 in DPBS) and incubated overnight at 4 °C. The mixture was then centrifuged at 17000g for 10 min at 4 °C. The pellet was collected and resuspended in DPBS containing trehalose (25 mM). The protein content in nanovesicles was quantified by Pierce BCA Protein Assay Kits (Thermo Scientific, USA), and the purified vesicles were stored at -80 °C for further use.

SEC Analysis. Superose 6 Increase 10/300 GL was pre-equilibrated with 0.01 M sodium phosphate (pH 7.2) using a Sepure SCG-100 chromatography station (Suzhou, China). 0.5 mL nanovesicles were loaded into the column and run at a flow rate of 0.5 mL/min.

Zeta Potential and Particle Size Distribution. The nanovesicles were diluted in water. The zeta potential and particle size of nanovesicles were determined by the Zetasizer Lab (Malvern Panalytical, England) according to the manufacturer's instructions.

Cryo-Transmission Electron Microscopy (Cryo-TEM). Two μ L of purified nanovesicles (1 mg/mL) was added to a glow-discharged Quantifoil holey carbon grid (Spi Supplies) and plunged into liquid ethane with Vitrobot Mark IV (Thermo Fisher, USA). The frozen grids were then transferred to a Glacios 200 kV field emission cryo transmission electron microscope (Thermo Fisher, USA). Images were recorded using a Falcon 4 director electron detector by a Ceta D CMOS camera (Thermo Fisher, USA).

Western Blotting. Membrane sheets and nanovesicles were lysed with a cell lysis buffer (Beyotime, P0013J). The concentration of protein was quantified by Pierce BCA Protein Assay Kits. Samples (20 μ g of total protein) were loaded into 4-20% sodium dodecyl sulfate polyacrylamide gels (ACE biotechnology, ET12420Gel) and electrophoresed at 120 V for 2 h. The protein on the gel was transferred to an immobilon P PVDF membrane (Millipore, IPVH00010). The membranes were blocked with 3% (weight/volume) BSA for 2 h at room temperature, followed by incubating with primary antibody (Na⁺/K⁺-ATPase rabbit mAb, ABclonal, A11683, 1:20,000; TSG101/VPS23 Rabbit pAb, ABclonal, A1692, 1:2000; Mouse anti DDDDK-Tag mAb, ABclonal, AE005, 1:5000; β -Actin mouse mAb, ABclonal, AC004, 1:20,000) at room temperature for 1 h and secondary antibody (HRP-conjugated goat anti-rabbit IgG (H + L), ABclonal, AS014, 1:10000; HRP-conjugated goat anti-mouse IgG (H + L), ABclonal, AS003, 1:10000) at room temperature for 1 h. After three times washing with TBST buffer, an enhanced chemiluminescent (ECL) HRP substrate (Proteintech, Catalog PK10001) was added, and chemiluminescence was detected using the ChemiDoc XRS + Gel imaging system (Bio-Rad).

Controlled Cargo Loading inside Vesicles. The isolated plasma membranes were reconstituted with DPBS at a concentration of 1 mg/mL, which was then mixed with the purified anti-actin nanobody-Nluc or anti-actin nanobody-sfGFP (5 μ M) at room temperature for 30 min. The mixture was centrifuged at 17000g for 1 h at 4 °C and then resuspended in DPBS. The procedure was repeated twice to completely remove the unbound tracers. The labeled membrane sheets were extruded into nanovesicles as in the method mentioned above.

Cell Viability Assay. HEK 293 cells were seeded in a 96-well plate at the density of 3000 cells per well. Twelve h later,

the nanovesicles were added into the wells by a series of dilutions ranging from 2000 to 10 $\mu\text{g}/\text{mL}$ (vesicle protein content conc.) The plate was returned to a cell culture incubator and incubated for 72 h. The CCK-8 reagent was added to the wells. After 2 h of incubation, the absorbance at 450 nm was measured by an Infinite M Plex microplate reader (TECAN, Switzerland). The cell viability was profiled using GraphPad Prism8 software.

Resistance to Protease Treatment. The anti-actin nanobody-Nluc-labeled HEK 293F vesicles (2.5 μg) were mixed with trypsin (serial dilution from 1250 to 0.125 $\text{ng}/\mu\text{L}$) at a final volume of 5 μL . The mixture was incubated at 37 $^{\circ}\text{C}$ for 5 min. The digestion reaction was stopped by adding 23 μL of BSA (200 $\mu\text{g}/\mu\text{L}$). A twenty-five μL portion of the Nano-Glo Luciferase Assay Substrate (Promega, N1110) was immediately added. Three minutes after incubation at room temperature, the luminescence intensity was measured by an Infinite M Plex microplate reader (TECAN, Switzerland).

Stability Test of Labeled Nanovesicles in Serum. One μg of anti-actin nanobody-NanoLuc labeled HEK 293F nanovesicles was mixed with mouse serum (final concentration 20%) at 37 $^{\circ}\text{C}$ for different time durations. The substrate was added to the samples and incubated for 3 min. The luminescence intensity was measured by an Infinite M Plex microplate reader (TECAN, Switzerland).

Protein Expression and Purification. The anti-actin nanobody-sfGFP and anti-actin nanobody-Nluc (sequences are available in Figure S4) were cloned into the pET-28a(+) vector. The plasmids were transformed into *Escherichia coli* Rosetta 2(DE3) cells (Millipore, USA). The strain was grown in the Luria–Bertani medium until the OD600 reached 0.6 to 0.8, and isopropyl β -D-thiogalactoside (IPTG) was added to the medium at a final concentration of 1 mM. Four hours later, the culture was harvested and resuspended in lysis buffer (20 mM Tris–HCl, pH 7.2, 1 M NaCl). The his \times 6 tagged protein was purified by Ni affinity chromatography, followed by ion exchange chromatography equipped with a HiScreen Q HP (Cytiva, Catalog 28950511) column. The purified protein was exchanged to PBS by a Sephadex G-25 desalting column and then stored at -80°C for further use.

Reprogramming HEK 293F Cells by Transient Transfection. The gene of scFv, derived from trastuzumab or cetuximab, was cloned into the pcDNA3.1 vector (Invitrogen, Catalog V79020). The insert was then in-frame with the CD8 α transmembrane region and signal peptide, respectively. The cysteines in the CD8 α hinge/transmembrane region were mutated to serine in order to eliminate dimerization.⁴ The amino acid sequences of the result CARs are listed in Figure S5. The day before transfection, HEK 293F cells were seeded at a density of 1.5×10^6 cells/mL in Union-293 media. In 10 mL of culture, 12.5 μg of the plasmid (diluted in 500 μL of Opti-MEM) and 40 μg of PEI MAX (Polysciences, Catalog 24765) (diluted in 500 μL of Opti-MEM) were mixed and incubated at 37 $^{\circ}\text{C}$ for 5 min. The mixture was added to the culture and shaken at a speed of 110 rpm at 37 $^{\circ}\text{C}$ in 5% CO_2 . Twenty h later, sodium butyrate (Beyotime, S1539-10g) was added to reach a final concentration of 10 mM. The CAR cells were harvested for PM purification 48 h after transfection.

Flow Cytometry. Calu-3 and HCC827 cells (25000 cells per well) were seeded in 24 wells overnight. To the cell culture medium was added 1 μg of CAR-free nanovesicles or CAR vesicles (labeled by anti-actin nanobody-sfGFP). Two hours after incubation at 37 $^{\circ}\text{C}$, the cell monolayer was digested with

trypsin (Gibco, 15050065) and cells were resuspended in DPBS. The fluorescence intensity of cells was analyzed by CytoFlex S (Beckman, USA) according to the manufacturer's instructions. To investigate the interaction specificity of CAR vesicles, the cells were pretreated with trastuzumab or cetuximab (100 nM) for 1 h to block the HER2 or EGFR receptors. The following uptake assay was performed in the presence of antibodies, as well. All data were processed with FlowJo 10.6.2.

Confocal Imaging. Calu-3 (10000 cells) were seeded in confocal dishes. After overnight culture, the culture was changed by 1 mL of fresh culture media (10% FBS), followed by adding 1 μg of anti-actin nanobody-sfGFP-labeled nanovesicles or CAR nanovesicles (the vesicle can be labeled by sulfo-Cy5 NHS). After incubation at 37 $^{\circ}\text{C}$ in 5% CO_2 (6, 12, and 24 h), Hoechst 33342 (Millipore Sigma, B2261) was added to stain the cell nucleus for 1 h at 37 $^{\circ}\text{C}$. The cell membrane was then counter-stained with WGA-AF 594 (Invitrogen, W11262) for 5 min. The monolayer was washed twice with DPBS and imaged with confocal laser scanning microscopy (Leica, USA).

Pharmacokinetic Studies of Nluc- or DiR-Labeled Nanovesicles. All of the animal studies were performed in compliance with the guidelines of the Chinese Regulations for the Administration of Affairs Concerning Experimental Animals and the Institutional Animal Care and Use Committee of Wuhan University. HEK 293F-derived nanovesicles were labeled with DiR (Bidepharm, BD450090) according to the user guide. The purified DiR-labeled nanovesicles were resuspended in DPBS and 100 μg of DiR or anti-actin nanobody-Nluc labeled nanovesicles were intravenously injected into the 6 to 8 week old BALB/c mice via the tail vein. Blood samples were collected at the indicated time points. The nanovesicles remaining in the blood sample were quantified by measuring the tracers' signal intensity, either NIR fluorescence (DiR) or bioluminescence (Nluc). For example, the DiR-labeled nanovesicles in the sample were measured by Odyssey DLX (LI-COR, USA), and data were analyzed by Image Studio Lite 5.2. As for the Nluc-labeled nanovesicles, the blood samples were mixed with a substrate and incubated for 3 min at room temperature. The luminescence was determined using a microplate reader (TECAN, Switzerland). The signal intensity of samples was normalized to that of the injected doses based on their relative fluorescence signals (RFU) or the Nluc luminescence. The pharmacokinetic profiles were expressed as a percentage of the injected dose/mL (% ID/mL) against time post-administration. Macrophage-depleted mice were prepared by intravenous injection of 200 μL of clodronate liposomes (SunLipo NanoTech, Catalog SN-ML-E005) according to a previous report.³⁷ 24 h later, 100 μg of anti-actin nanobody-Nluc-labeled vesicles were intravenously injected via the tail vein. Blood samples were collected at indicated time points. The samples were analyzed using the methods mentioned above.

Bioluminescence Imaging In Vivo. The Calu-3 xenograft tumor model was established by subcutaneous injection of Calu-3 cells (5×10^6) to the dorsal of 8 week-old BALB/c-nu mice. The tumor volume was measured 2 times per week, and the size was calculated using the formula $\text{length} \times \text{width}^2/2$. The in vivo imaging study was performed when the tumor volume reached 500 mm^3 . DiR or anti-actin nanobody-Nluc-labeled nanovesicles (100 μg) were intravenously injected into mice via the tail vein. At the indicated time points, mice of the

DiR nanovesicle group were imaged using the In-Vivo Xtreme II imaging system (Bruker, USA). As for mice injected with anti-actin nanobody-Nluc-labeled nanovesicles, the substrate was injected 3 min before imaging. For ex vivo imaging, organs were dissected and imaged at the indicated time points. For lysate quantification, organs were cut into pieces with surgical scissors, and DPBS was added to reach 5 mL/g. The tissues were homogenized with a hand-held tissue homogenizer (HUXI, HR-6B). A 50 μ L portion of lysate was used to determine the RFU. To quantify bioluminescence in groups of anti-actin Nb-Nluc-labeled nanovesicles, 25 μ L of the homogenate was mixed with the substrate and then measured by a microplate reader. The remaining vesicles in samples were expressed as RFU/g tissue (RFU/gT) and luminescence/g tissue (RLU/gT).

Statistical Analysis. Statistical analysis was performed using GraphPad Prism 9.3.0, data were presented as mean \pm standard deviation, *P*-values were calculated using the two-way ANOVA with Tukey's multiple comparison test, and *P* < 0.05 was considered to be statistically significant.

■ ASSOCIATED CONTENT

SI Supporting Information

The Supporting Information is available free of charge at <https://pubs.acs.org/doi/10.1021/acs.molpharmaceut.4c00927>.

SEC spectra of nanovesicles; PM images; additional cryo-TEM images of vesicles; semi-quantitative data of β -actin in Western blotting images; flow cytometric charts; fusion proteins' sequences; and SDS-PAGE characterization (PDF)

■ AUTHOR INFORMATION

Corresponding Author

Wanyi Tai – Department of Pharmaceutical Engineering, School of Pharmaceutical Sciences, Wuhan University, Wuhan, Hubei 430071, China; orcid.org/0000-0003-3589-8263; Email: wanyi-tai@whu.edu.cn

Authors

Yahui Liu – Department of Pharmaceutical Engineering, School of Pharmaceutical Sciences, Wuhan University, Wuhan, Hubei 430071, China

Yuele Ling – Department of Pharmaceutical Engineering, School of Pharmaceutical Sciences, Wuhan University, Wuhan, Hubei 430071, China

Complete contact information is available at:

<https://pubs.acs.org/doi/10.1021/acs.molpharmaceut.4c00927>

Notes

The authors declare no competing financial interest.

■ ACKNOWLEDGMENTS

This work was financially supported by the National Key R&D Program of China (Grant No. 2021YFA0909900) and the National Natural Science Foundation of China (Grant Nos. 82073770 and 82273860).

■ REFERENCES

- (1) Cheng, C.-A. Before Translating Extracellular Vesicles into Personalized Diagnostics and Therapeutics: What We Could Do. *Mol. Pharmaceutics* **2024**, *21* (6), 2625–2636.
- (2) Rashed, M. H.; Bayraktar, E.; Helal, G. K.; Abd-Ellah, M. F.; Amero, P.; Chavez-Reyes, A.; Rodriguez-Aguayo, C. Exosomes: From Garbage Bins to Promising Therapeutic Targets. *Int. J. Mol. Sci.* **2017**, *18* (3), 538.
- (3) Meldolesi, J. Exosomes and Ectosomes in Intercellular Communication. *Curr. Biol.* **2018**, *28* (8), R435–r444.
- (4) van Niel, G.; D'Angelo, G.; Raposo, G. Shedding light on the cell biology of extracellular vesicles. *Nat. Rev. Mol. Cell Biol.* **2018**, *19* (4), 213–228.
- (5) Zhu, X.; Badawi, M.; Pomeroy, S.; Sutaria, D. S.; Xie, Z.; Baek, A.; Jiang, J.; Elgamel, O. A.; Mo, X.; La Perle, K.; Chalmers, J.; Schmittgen, T. D.; Phelps, M. A. Comprehensive toxicity and immunogenicity studies reveal minimal effects in mice following sustained dosing of extracellular vesicles derived from HEK293T cells. *J. Extracell. Vesicles* **2017**, *6* (1), 1324730.
- (6) Zhuang, X.; Xiang, X.; Grizzle, W.; Sun, D.; Zhang, S.; Axtell, R. C.; Ju, S.; Mu, J.; Zhang, L.; Steinman, L.; Miller, D.; Zhang, H. G. Treatment of brain inflammatory diseases by delivering exosome encapsulated anti-inflammatory drugs from the nasal region to the brain. *Mol. Ther.* **2011**, *19* (10), 1769–1779.
- (7) Lu, M.; Huang, Y. Bioinspired exosome-like therapeutics and delivery nanoplatfoms. *Biomaterials* **2020**, *242*, 119925.
- (8) Morishita, M.; Takahashi, Y.; Matsumoto, A.; Nishikawa, M.; Takakura, Y. Exosome-based tumor antigens-adjuvant co-delivery utilizing genetically engineered tumor cell-derived exosomes with immunostimulatory CpG DNA. *Biomaterials* **2016**, *111*, 55–65.
- (9) Gee, P.; Lung, M. S. Y.; Okuzaki, Y.; Sasakawa, N.; Iguchi, T.; Makita, Y.; Hozumi, H.; Miura, Y.; Yang, L. F.; Iwasaki, M.; Wang, X. H.; Waller, M. A.; Shirai, N.; Abe, Y. O.; Fujita, Y.; Watanabe, K.; Kagita, A.; Iwabuchi, K. A.; Yasuda, M.; Xu, H.; Noda, T.; Komano, J.; Sakurai, H.; Inukai, N.; Hotta, A. Extracellular nanovesicles for packaging of CRISPR-Cas9 protein and sgRNA to induce therapeutic exon skipping. *Nat. Commun.* **2020**, *11* (1), 1334.
- (10) Lu, Y.; Godbout, K.; Lamothe, G.; Tremblay, J. P. CRISPR-Cas9 delivery strategies with engineered extracellular vesicles. *Mol. Ther. Nucleic Acids* **2023**, *34*, 102040.
- (11) Rezaie, J.; Feghhi, M.; Etemadi, T. A review on exosomes application in clinical trials: perspective, questions, and challenges. *Cell Commun. Signal.* **2022**, *20* (1), 145.
- (12) Lotfy, A.; AboQuella, N. M.; Wang, H. Mesenchymal stromal/stem cell (MSC)-derived exosomes in clinical trials. *Stem Cell Res. Ther.* **2023**, *14* (1), 66.
- (13) Dehghani, L.; Khojasteh, A.; Soleimani, M.; Oraee-Yazdani, S.; Keshel, S. H.; Saadatnia, M.; Saboori, M.; Zali, A.; Hashemi, S. M.; Soleimani, R. Safety of Intraparenchymal Injection of Allogenic Placenta Mesenchymal Stem Cells Derived Exosome in Patients Undergoing Decompressive Craniectomy Following Malignant Middle Cerebral Artery Infarct, A Pilot Randomized Clinical Trial. *Int. J. Prev. Med.* **2022**, *13*, 7.
- (14) Surana, R.; LeBleu, V. S.; Lee, J. J.; Smaglo, B. G.; Zhao, D.; Lee, M. S.; Wolff, R. A.; Overman, M. J.; Mendt, M. C.; McAndrews, K. M.; Yang, S.; Rezvani, K.; Kalluri, R.; Maitra, A.; Shpall, E. J.; Pant, S. Phase I study of mesenchymal stem cell (MSC)-derived exosomes with KRASG12D siRNA in patients with metastatic pancreatic cancer harboring a KRASG12D mutation. *J. Clin. Oncol.* **2022**, *40* (4_suppl), TPS633.
- (15) Wang, Z.; Zhou, X.; Kong, Q.; He, H.; Sun, J.; Qiu, W.; Zhang, L.; Yang, M. Extracellular Vesicle Preparation and Analysis: A State-of-the-Art Review. *Adv. Sci.* **2024**, *11*, No. e2401069.
- (16) Kimiz-Gebologlu, I.; Oncel, S. S. Exosomes: Large-scale production, isolation, drug loading efficiency, and biodistribution and uptake. *J. Controlled Release* **2022**, *347*, 533–543.
- (17) Herrmann, I. K.; Wood, M. J. A.; Fuhrmann, G. Extracellular vesicles as a next-generation drug delivery platform. *Nat. Nanotechnol.* **2021**, *16* (7), 748–759.
- (18) Mathieu, M.; Névo, N.; Jouve, M.; Valenzuela, J. I.; Maurin, M.; Verweij, F. J.; Palmulli, R.; Lankar, D.; Dingli, F.; Loew, D.; Rubinstein, E.; Boncompain, G.; Perez, F.; Théry, C. Specificities of

exosome versus small ectosome secretion revealed by live intracellular tracking of CD63 and CD9. *Nat. Commun.* **2021**, *12* (1), 4389.

(19) Cocucci, E.; Meldolesi, J. Ectosomes and exosomes: shedding the confusion between extracellular vesicles. *Trends Cell Biol.* **2015**, *25* (6), 364–372.

(20) Soares Martins, T.; Catita, J.; Martins Rosa, I.; da Cruz e Silva, O. A. B.; Henriques, A. G. Exosome isolation from distinct biofluids using precipitation and column-based approaches. *PLoS One* **2018**, *13* (6), No. e0198820.

(21) Chen, Y.; Zhu, Q.; Cheng, L.; Wang, Y.; Li, M.; Yang, Q.; Hu, L.; Lou, D.; Li, J.; Dong, X.; Lee, L. P.; Liu, F. Exosome detection via the ultrafast-isolation system: EXODUS. *Nat. Methods* **2021**, *18* (2), 212–218.

(22) Brennan, K.; Martin, K.; FitzGerald, S. P.; O'Sullivan, J.; Wu, Y.; Blanco, A.; Richardson, C.; Mc Gee, M. M. A comparison of methods for the isolation and separation of extracellular vesicles from protein and lipid particles in human serum. *Sci. Rep.* **2020**, *10* (1), 1039.

(23) Patel, G. K.; Khan, M. A.; Zubair, H.; Srivastava, S. K.; Khushman, M. d.; Singh, S.; Singh, A. P. Comparative analysis of exosome isolation methods using culture supernatant for optimum yield, purity and downstream applications. *Sci. Rep.* **2019**, *9* (1), 5335.

(24) Baranyai, T.; Herczeg, K.; Onódi, Z.; Voszka, I.; Módos, K.; Marton, N.; Nagy, G.; Mäger, L.; Wood, M. J.; El Andaloussi, S.; Pálincás, Z.; Kumar, V.; Nagy, P.; Kittel, A.; Buzás, E. I.; Ferdinandy, P.; Giricz, Z. Isolation of Exosomes from Blood Plasma: Qualitative and Quantitative Comparison of Ultracentrifugation and Size Exclusion Chromatography Methods. *PLoS One* **2015**, *10* (12), No. e0145686.

(25) Coughlan, C.; Bruce, K. D.; Burgy, O.; Boyd, T. D.; Michel, C. R.; Garcia-Perez, J. E.; Adame, V.; Anton, P.; Bettcher, B. M.; Chial, H. J.; Königshoff, M.; Hsieh, E. W. Y.; Graner, M.; Potter, H. Exosome Isolation by Ultracentrifugation and Precipitation and Techniques for Downstream Analyses. *Curr. Protoc. Cell Biol.* **2020**, *88* (1), No. e110.

(26) Wu, H.; Oliver, A. E.; Ngassam, V. N.; Yee, C. K.; Parikh, A. N.; Yeh, Y. Preparation, characterization, and surface immobilization of native vesicles obtained by mechanical extrusion of mammalian cells. *Integr. Biol.* **2012**, *4* (6), 685–692.

(27) Lunavat, T. R.; Jang, S. C.; Nilsson, L.; Park, H. T.; Repiska, G.; Lässer, C.; Nilsson, J. A.; Gho, Y. S.; Lötvall, J. RNAi delivery by exosome-mimetic nanovesicles - Implications for targeting c-Myc in cancer. *Biomaterials* **2016**, *102*, 231–238.

(28) Jo, W.; Kim, J.; Yoon, J.; Jeong, D.; Cho, S.; Jeong, H.; Yoon, Y. J.; Kim, S. C.; Gho, Y. S.; Park, J. Large-scale generation of cell-derived nanovesicles. *Nanoscale* **2014**, *6* (20), 12056–12064.

(29) Jang, S. C.; Kim, O. Y.; Yoon, C. M.; Choi, D. S.; Roh, T. Y.; Park, J.; Nilsson, J.; Lötvall, J.; Kim, Y. K.; Gho, Y. S. Bioinspired exosome-mimetic nanovesicles for targeted delivery of chemotherapeutics to malignant tumors. *ACS Nano* **2013**, *7* (9), 7698–7710.

(30) Shingles, R.; McCarty, R. E. Production of membrane vesicles by extrusion: size distribution, enzyme activity, and orientation of plasma membrane and chloroplast inner-envelope membrane vesicles. *Anal. Biochem.* **1995**, *229* (1), 92–98.

(31) Koziel, K.; Lebieczinska, M.; Szabadkai, G.; Onopiuk, M.; Brutkowski, W.; Wierzbicka, K.; Wilczyński, G.; Pinton, P.; Duszyński, J.; Zabłocki, K.; Wieckowski, M. R. Plasma membrane associated membranes (PAM) from Jurkat cells contain STIM1 protein. *Int. J. Biochem. Cell Biol.* **2009**, *41* (12), 2440–2449.

(32) Suski, J. M.; Lebieczinska, M.; Wojtala, A.; Duszyński, J.; Giorgi, C.; Pinton, P.; Wieckowski, M. R. Isolation of plasma membrane-associated membranes from rat liver. *Nat. Protoc.* **2014**, *9* (2), 312–322.

(33) Rider, M. A.; Hurwitz, S. N.; Meckes, D. G. ExtraPEG: A Polyethylene Glycol-Based Method for Enrichment of Extracellular Vesicles. *Sci. Rep.* **2016**, *6* (1), 23978.

(34) Ludwig, A. K.; De Miroschedji, K.; Doepfner, T. R.; Börger, V.; Ruesing, J.; Rebmann, V.; Durst, S.; Jansen, S.; Bremer, M.;

Behrmann, E.; Singer, B. B.; Jastrow, H.; Kuhlmann, J. D.; El Magraoui, F.; Meyer, H. E.; Hermann, D. M.; Opalka, B.; Raunser, S.; Eppl, M.; Horn, P. A.; Giebel, B. Precipitation with polyethylene glycol followed by washing and pelleting by ultracentrifugation enriches extracellular vesicles from tissue culture supernatants in small and large scales. *J. Extracell. Vesicles* **2018**, *7* (1), 1528109.

(35) Vickers, K. C.; Palmisano, B. T.; Shoucri, B. M.; Shamburek, R. D.; Remaley, A. T. MicroRNAs are transported in plasma and delivered to recipient cells by high-density lipoproteins. *Nat. Cell Biol.* **2011**, *13* (4), 423–433.

(36) Kooijmans, S. A. A.; Vader, P.; Schiffelers, R. M. Tumour-bound RNA-laden exosomes. *Nat. Biomed. Eng.* **2017**, *1* (8), 634–636.

(37) Imai, T.; Takahashi, Y.; Nishikawa, M.; Kato, K.; Morishita, M.; Yamashita, T.; Matsumoto, A.; Charoenviriyakul, C.; Takakura, Y. Macrophage-dependent clearance of systemically administered B16BL6-derived exosomes from the blood circulation in mice. *J. Extracell. Vesicles* **2015**, *4*, 26238.

(38) Liam-Or, R.; Faruqi, F. N.; Walters, A.; Han, S.; Xu, L.; Wang, J. T.-W.; Oberlaender, J.; Sanchez-Fueyo, A.; Lombardi, G.; Dazzi, F.; Mailaender, V.; Al-Jamal, K. T. Cellular uptake and in vivo distribution of mesenchymal-stem-cell-derived extracellular vesicles are protein corona dependent. *Nat. Nanotechnol.* **2024**, *19* (6), 846–855.

(39) Smyth, T.; Kullberg, M.; Malik, N.; Smith-Jones, P.; Graner, M. W.; Anchordoquy, T. J. Biodistribution and delivery efficiency of unmodified tumor-derived exosomes. *J. Controlled Release* **2015**, *199*, 145–155.

(40) Lázaro-Ibáñez, E.; Faruqi, F. N.; Saleh, A. F.; Silva, A. M.; Tzu-Wen Wang, J.; Rak, J.; Al-Jamal, K. T.; Dekker, N. Selection of Fluorescent, Bioluminescent, and Radioactive Tracers to Accurately Reflect Extracellular Vesicle Biodistribution in Vivo. *ACS Nano* **2021**, *15* (2), 3212–3227.

(41) Charoenviriyakul, C.; Takahashi, Y.; Morishita, M.; Nishikawa, M.; Takakura, Y. Role of Extracellular Vesicle Surface Proteins in the Pharmacokinetics of Extracellular Vesicles. *Mol. Pharmaceutics* **2018**, *15* (3), 1073–1080.

(42) Hoshino, A.; Costa-Silva, B.; Shen, T.-L.; Rodrigues, G.; Hashimoto, A.; Tesic Mark, M.; Molina, H.; Kohsaka, S.; Di Giannatale, A.; Ceder, S.; Singh, S.; Williams, C.; Soplop, N.; Uryu, K.; Pharmed, L.; King, T.; Bojmar, L.; Davies, A. E.; Ararso, Y.; Zhang, T.; Zhang, H.; Hernandez, J.; Weiss, J. M.; Dumont-Cole, V. D.; Kramer, K.; Wexler, L. H.; Narendran, A.; Schwartz, G. K.; Healey, J. H.; Sandstrom, P.; Jørgen Labori, K.; Kure, E. H.; Grandgenett, P. M.; Hollingsworth, M. A.; de Sousa, M.; Kaur, S.; Jain, M.; Mallya, K.; Batra, S. K.; Jarnagin, W. R.; Brady, M. S.; Fodstad, O.; Muller, V.; Pantel, K.; Minn, A. J.; Bissell, M. J.; Garcia, B. A.; Kang, Y.; Rajasekhar, V. K.; Ghajar, C. M.; Matei, I.; Peinado, H.; Bromberg, J.; Lyden, D. Tumour exosome integrins determine organotropic metastasis. *Nature* **2015**, *527* (7578), 329–335.

(43) Mammadova-Bach, E.; Zigrino, P.; Brucker, C.; Bourdon, C.; Freund, M.; De Arcangelis, A.; Abrams, S. I.; Orend, G.; Gachet, C.; Mangin, P. H. Platelet integrin $\alpha 6 \beta 1$ controls lung metastasis through direct binding to cancer cell-derived ADAM9. *JCI insight* **2016**, *1* (14), No. e88245.

(44) Severic, M.; Ma, G.; Pereira, S. G. T.; Ruiz, A.; Cheung, C. C. L.; Al-Jamal, W. T. Genetically-engineered anti-PSMA exosome mimetics targeting advanced prostate cancer in vitro and in vivo. *J. Controlled Release* **2021**, *330*, 101–110.

(45) Cunha, L. M.; Bernardino-Neto, M.; Garrote-Filho, M. d. S.; Avelar, C. B.; de Freitas, M. V.; Mascarenhas Netto, R. d. C.; Paraiso, L. F.; de Arvelos, L. R.; Gonçalves-e-Oliveira, A. F. M.; Penha-Silva, N. Kinetics of hypotonic lysis of human erythrocytes. *Anal. Methods* **2014**, *6* (5), 1377–1383.